RSC Advances

ROYAL SOCIETY OF CHEMISTRY

www.rsc.org/advances

RSC Advances

ARTICLE

Remarkable Flux Effect of Li-Codoping on Highly Enhanced Luminescence of Orthosilicate Phosphors, $Ba_2SiO_4:Eu^{2+}$ for NUV-LEDs: Autonomous Impurity Purification by Eutectic Li_2CO_3 Melts

Received 00th January 20xx,
Accepted 00th January 20xx

DOI: 10.1039/x0xx00000x

www.rsc.org/

Donghyeon Kim,[a] Ki-Wan Jeon,[c] Jong Sung Jin,[d] Seong-Gu Kang,[e] Dong-Kyun Seo[c] and Jung-Chul Park[*ab]

We report large photoluminescence (PL) enhancement of green-emitting $Ba_2SiO_4:Eu^{2+}$ phosphor prepared in an eutectic Li_2CO_3 melt as a flux. Among the phosphor materials synthesized using low-purity precursors (99%-pure $BaCO_3$ and 99.6%-pure SiO_2), the emission intensity of $Ba_2SiO_4:(Li_{0.02},Eu_{0.02})$ (Li = 200% excess) is found to be 470% as high as that of $Ba_2SiO_4:Eu_{0.02}$ (no-Li) and in fact is almost equivalent to that of Li-undoped $Ba_2SiO_4:Eu^{2+}$ synthesized using ultrapure precursors (99.98%-pure $BaCO_3$ and 99.995%-pure SiO_2). In combination with the results from PL measurements and inductively coupled plasma mass spectrometry (ICP-MS), the elemental distribution of the products and melts found from time-of-flight secondary ion mass spectrometry (TOF-SIMS) directly indicates that the excess Li_2CO_3 autonomously removes the impurities that were originally contained in the low-purity precursors, in particular SiO_2, and thus critically improves the photoluminescence efficiency of the material. The newly found Li flux effect of large PL enhancement may not only contribute to more economic production of phosphors but provide a platform in discovery of new efficient phosphors for solid state lighting.

1 Introduction

In search for highly efficient solid state lighting materials, Li-codoping have been very successful in improving luminescence properties of rare earth-doped phosphors.[1-12] It is generally accepted that the Li^+ ions doped in the host lattices play important roles in the enhanced luminescent property of phosphors. The enhanced luminescence of the Li-codoped phosphors has been explained, as follows: i) copresence of Li^+ ions favorably modifies the local structure of the activator ions and their special distribution;[1-4] ii) codoping of Li^+ ions creates oxygen vacancies which might act as a sensitizer for the energy transfer to activator ions;[5,7,9,10] iii) Li precursors such as Li_2CO_3 or LiF act as a flux which promotes incorporation of the activator ions into the host lattice and also enhances crystal growth during the firing process at high temperatures;[5,6,12] and iv) Li-codoping provides to the product particles a morphology that is more desirable in reducing internal reflection.[5,6] Among those possible mechanisms of the luminescence enhancement by Li-codoping, the flux effect (i.e., iii)) has been found to play a minor role. In the studies of Li-codoping in $Y_2SiO_5:Pr^{3+}$,[12] for example, the flux effect was responsible to ~5% of the total enhancement of the emission, while the structural effect including increased Pr^{3+} separation and phase change was accountable for the rest (95%). Herein we report that the flux effect can be much more significant via a newly discovered mechanism, that is, autonomous impurity purification, by using green-emitting $(Ba,Sr)_2SiO_4:Eu^{2+}$ phosphor system. Green-emitting $(Ba,Sr)_2SiO_4:Eu^{2+}$ phosphor is promising for UV-LEDs because of its short decay time and high luminescence characteristics under UV excitation. Furthermore, the chromaticity of the $(Ba,Sr)_2SiO_4:Eu$ phosphor can be controlled from the near UV (NUV) to the red by changing the crystal field splitting or covalency of the host lattice through Li-codoping, for example.[13,14] The electronic configuration of Eu^{2+} is $[Xe]4f^7$, and its lowest excited state of 4f levels is located at 28×10^3 cm^{-1} and it is in higher energy than that of the $4f^65d^1$ in most compounds, so that Eu^{2+} usually exhibits broad-band emission associated with f-d transitions. As the Eu^{2+} activator is incorporated in Ba^{2+} sites, a new interaction between $[SiO_4]^{4-}$ and Eu^{2+} activator probably occurs, -[O-Si-O]−Eu^{2+}−[O-Si-O]-. Thus, by Li^+ codoping, the change of covalency as well as crystal field strength in the host lattice may give rise to the modification of the characteristic of Eu^{2+} emission, which results in the improved luminescent intensity of $Ba_2SiO_4:Eu^{2+}$ phosphor. Additional Li-codoping effect has not been reported so far in enhancing the luminescent property of the phosphors or for Eu^{2+}-activated phosphors in general, although such

[a] Graduate School of Advanced Engineering, Silla University, Busan 617-736, Republic of Korea. E-mail: parkjc@silla.ac.kr
[b] Center for Green Fusion Technology and Department of Engineering in Energy & Applied Chemistry, Silla University, Busan617-736, Republic of Korea
[c] Department of Chemistry and Biochemistry, Arizona State University, Tempe, AZ 85287-1604, USA
[d] Busan Center, Korea Basic Science Institute, Busan 618-230, Republic of Korea
[e] Department of Chemical Engineering, Hoseo University, Asan-Si, Chungnam-Do, 336-795, Republic of Korea

enhancement from a flux effect for Eu^{2+}-activated phosphors have been discovered by one of the authors.[5,6]

2 Experimental

Li-codoped $Ba_2SiO_4:Eu^{2+}$ materials were synthesized via a solid-state reaction with stoichiometric or excessive amounts of Li_2CO_3. The stoichiometric amounts of $BaCO_3$ (Aldrich, 99% and 99.98%), SiO_2 (Aldrich, 99.6% and 99.995%) Li_2CO_3 (Aldrich, 99.99%), and Eu_2O_3 (Aldrich, 99.9%) were mixed and pulverized, then heated at 1250℃ for 6h in air using alumina boats for the regular syntheses. The obtained powders with white body color were fired at 1250℃ for 6h in mild reducing atmosphere (4% H_2/Ar). After the reduction of the material, the white colored powder was changed into a white-greenish powder. Additionally, in the weighing step, Li_2CO_3 was added excessively between 100 and 300% excess relative to the stoichiometric one. Thermogravimetry and differential scanning calorimetry (TG/DSC, SDT Q 600 model) were used to determine the weight loss of starting materials, such as $BaCO_3$, SiO_2, Eu_2O_3, and Li_2CO_3. A heating rate of 10℃/min was used for measurements from room temperature to 1200℃ in air. The structures of Ba_2SiO_4:(Li,Eu) compounds were characterized using a X-ray diffractometer (XRD 6000 model, Shimadzu) using Cu-Kα radiation at 30 kV and 30 mA. The unit-cell parameters were obtained using a nonlinear least-squares cell refinement program (UnitCell). The luminescent spectra were measured at room temperature using a fluorescent spectrophotometer (Scinco, FluoroMate FS-2). The reflectance spectra of phosphors were recorded using UV-visible spectrophotometer (UV-2600, Shimadzu) with $BaSO_4$ as a reference. Elemental analysis was performed using an inductively coupled plasma mass spectrometer (ICP-MS, ELAN DRC II model, Perkin Elmer). TOF-SIMS experiments were performed with a TOF-SIMS V (ION-TOF GmbH, Münster, Germany) instrument in KBSI, Busan center by using a pulsed 30 keV Bi^+ primary beam with a current 1 pA. The analyzed area used in this work was a square of 100 μm × 100 μm and the data acquisition time was 100 s. In order to prepare SIMS samples, the high purity indium metal (99.995% purity) was cut and pressed loosely using a pelletizer (ϕ = 8 mm), and subsequently the powder sample was placed over the indium metal disc and pressed. The particulates were homogeneously embedded in the indium metal disc. Positive ion spectra were internally calibrated using H^+, H^{2+}, CH_3^+, $C_2H_5^+$, and $C_3H_7^+$ peaks and normalized to the respective secondary total ion yields. The chemical images of the analyzed area were recorded with 128×128 pixel resolution during the data acquisition. Charge effects were compensated by means of an interlaced pulsed electron flood gun (E_k = 20 eV). The brightness of phosphor materials was measured using a CHROMA METER CS-100A model (MINOLTA). PL quantum yields of $Ba_2SiO_4:Eu_{0.02}$ phosphor materials before and after Li-doping were measured using a PL spectrometer with an integrating sphere (Hamamatsu Photonics: Quantum Yield Measurement system C9920-02) at room temperature.

3 Results and discussion

3.1 TG/DSC of Li-Compounds as a Li^+-Ion Source and Structural Characterization.

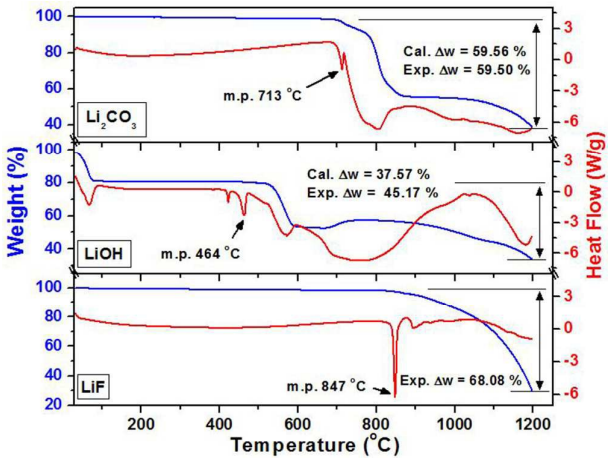

Fig. 1 TG and DSC curves of Li_2CO_3, LiOH, and LiF.

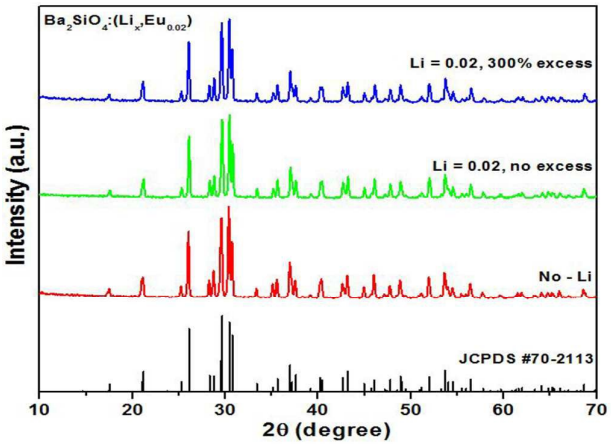

Fig. 2 XRD patterns of Ba2SiO4:(Li,Eu) phosphors.

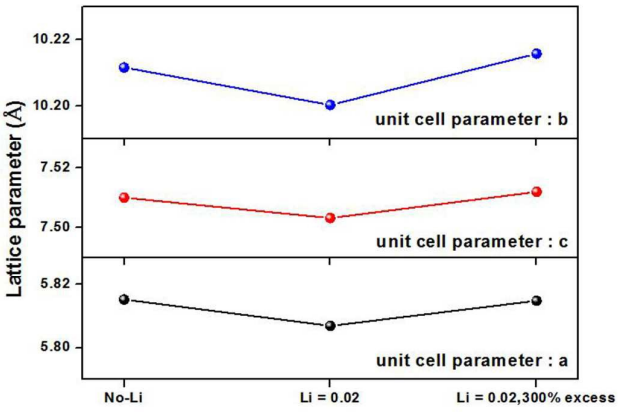

Fig. 3 Variation of unit cell parameters in Ba_2SiO_4:(Li,Eu) phosphors as a function of Li content.

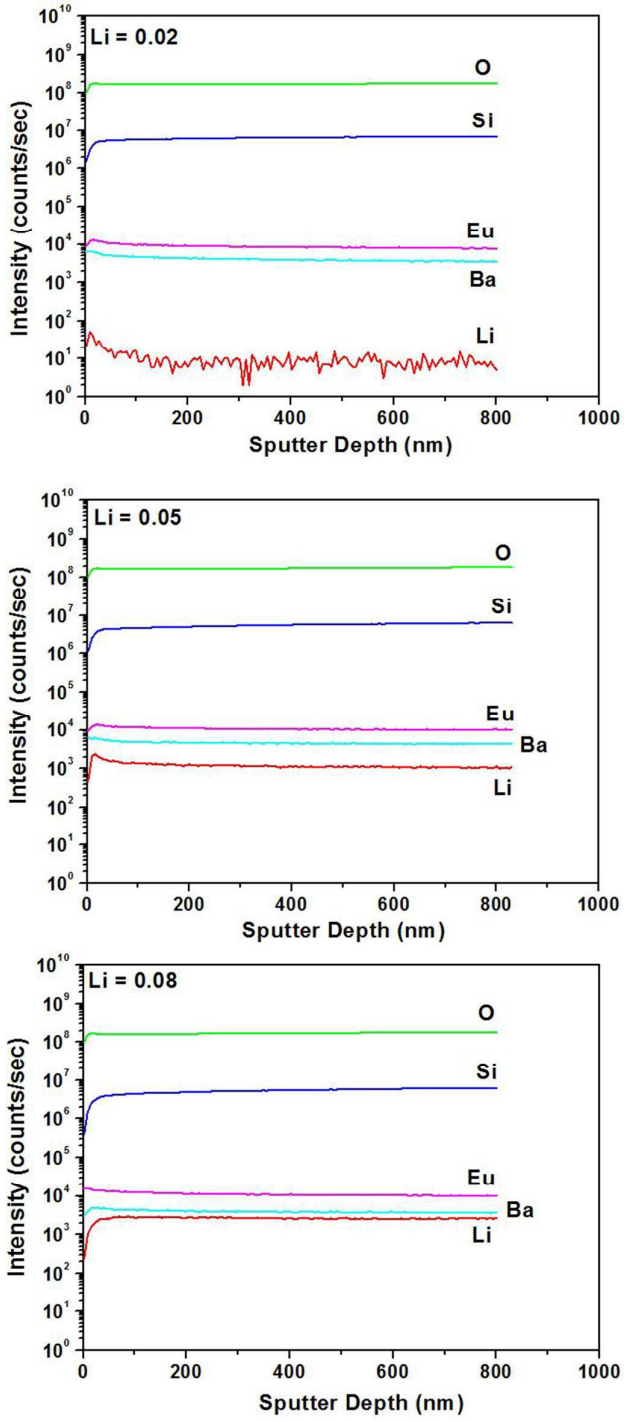

Fig. 4 Atomic intensity versus sputtered depth of $Ba_2SiO_4:(Li_x,Eu_{0.02})$ as a function of Li content.

TG and DSC were performed to examine the thermal behavior of the Li_2CO_3, LiOH, and LiF as a Li^+-ion source as shown in Fig. 1. The additional TG/DSC curves of $BaCO_3$, SiO_2, and Eu_2O_3 are presented in Fig. S1 (Supporting Information). The weight loss of Li_2CO_3 begins at around 700℃ and is complete at 800℃ with the melting point at 713℃ in DSC curve and subsequently the additional weight loss restarts up to 1200℃ corresponding to the decarbonation of Li_2CO_3, in which the experimental weight loss (59.5%) is in good agreement with the theoretical value (59.6%). For Li_2O, the continuous weight loss above 1000℃ may be due to slow evaporation of Li_2O. LiOH dehydroxyates to form Li_2O above ~500℃ and the formed Li_2O gradually evaporates at the high temperature region. However, the origin of the slight weight gain between 680 and 960℃ is not clear. The TG thermogram of LiF indicates that evaporation of LiF starts at ~840℃ and is significant in our firing condition (at 1250 ℃ for 6h in air). Based on the TG and DSC thermograms, therefore, Li_2CO_3 is the best candidate as a Li^+-ion source in examining the Li-doping effect of the host materials. The X-ray diffraction (XRD) patterns of three products with different amounts of Li_2CO_3 are shown in Fig. 2 and they are consistent with the XRD pattern of Ba_2SiO_4 with a primitive orthorhombic cell (*Pmcn*).[15] The refined unit cell parameters are as follows: for $Ba_2SiO_4:Eu_{0.02}$ (no-Li), a = 5.815 Å, b = 10.211 Å, c = 7.510 Å; for $Ba_2SiO_4:(Li_{0.02},Eu_{0.02})$ (nominal-Li), a = 5.807 Å, b = 10.200 Å, c = 7.503 Å; and for $Ba_2SiO_4:(Li_{0.02},Eu_{0.02})$ (Li-300% excess), a = 5.815 Å, b = 10.216 Å, c = 7.512 Å. It is noted that the unit cell parameters of the Li doped compound, $Ba_2SiO_4:(Li_{0.02},Eu_{0.02})$ (nominal-Li) are slightly reduced compared with those of $Ba_2SiO_4:Eu_{0.02}$ (no-Li), which is probably due to the formation of the oxygen defects associated with the volatility of Li_2O at high temperature. At a higher Li doping level (300% excess), the unit cell parameters are close to those of $Ba_2SiO_4:Eu_{0.02}$ (no-Li) compound as shown in Fig. 3. SIMS studies were carried out in order to examine the content of Li as well as other elements present,[16,17] and the depth profile of secondary ion intensities (for Ba, Si, Eu, Li, and O atom) of $Ba_2SiO_4:(Li_x,Eu_{0.02}$; x = 0.02, 0.05 and 0.08) are shown in Fig. 4. The sample with a larger Li content shows a larger signal intensity in the Li channel and somewhat smaller intensity for the Ba while the rest of the elements (Si, and O) have the nearly the same intensities. Evidently, the SIMS intensity of Ba is gradually diminished with increasing Li-content because Li-ions occupy Ba sites in the Ba_2SiO_4 crystal lattice with an orthosilicate-type structure as depicted in $Ba_{2-x}Li_xO_4$ chemical formula. In addition, the signal intensities of the elements are constant from near the surface to the interior (ca. 800 nm) of the grains for all the samples, indicating that the individual particles are atomistically homogeneous throughout the body, as desired.

3.2 Photoluminescence Spectra of Li-doped $Ba_2SiO_4:Eu_{0.02}$ Materials.

Fig. 5 shows the PL spectra and emission spectra (λ_{ex} = 370 nm) of $Ba_2SiO_4:Eu_{0.02}$ and its Li-codoped samples synthesized using $BaCO_3$ (99% purity), SiO_2 (99.6% purity), Eu_2O_3 (99.9% purity) and Li_2CO_3 (99.99% purity), in which x is the nominal amount of Li (x = 0.02, 0.05 and 0.08). All the samples exhibit a broad absorption band from 220 to 470 nm, which may be ascribed to the spin allowed $4f^7(^8S_{2/7})$–$4f^65d$ transitions of Eu^{2+}.[18-22] The emission spectra show symmetric bands centered at 503 nm, associated with a green-emission. The emission

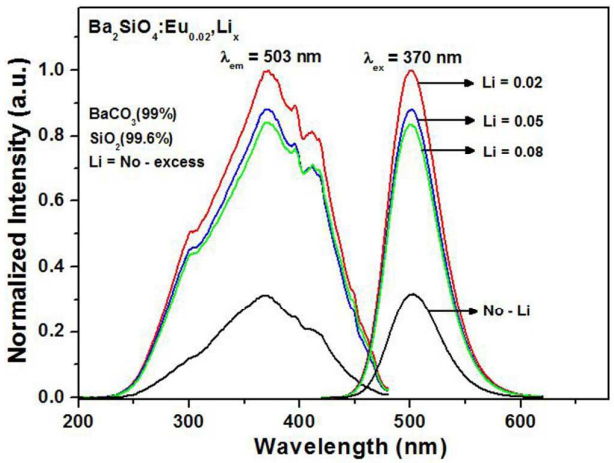

Fig. 5 PL spectra of Ba_2SiO_4:(Li_x,$Eu_{0.02}$) as a function of Li content.

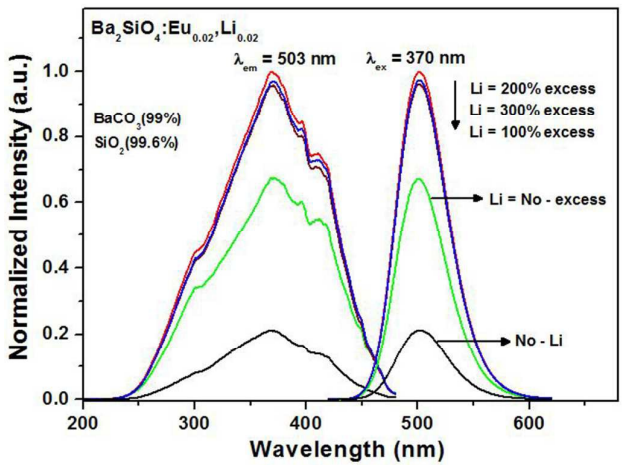

Fig. 7 PL spectra of Ba_2SiO_4:($Li_{0.02}$,$Eu_{0.02}$) synthesized with Li-excess.

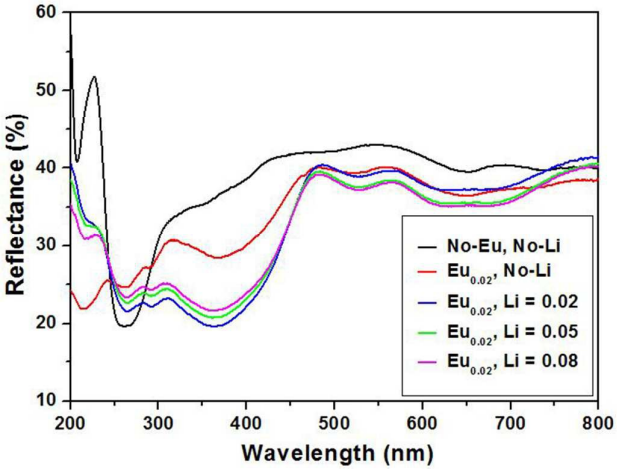

Fig. 6 Diffuse reflectance spectra of Ba_2SiO_4:(Li_x,$Eu_{0.02}$) as a function of Li content.

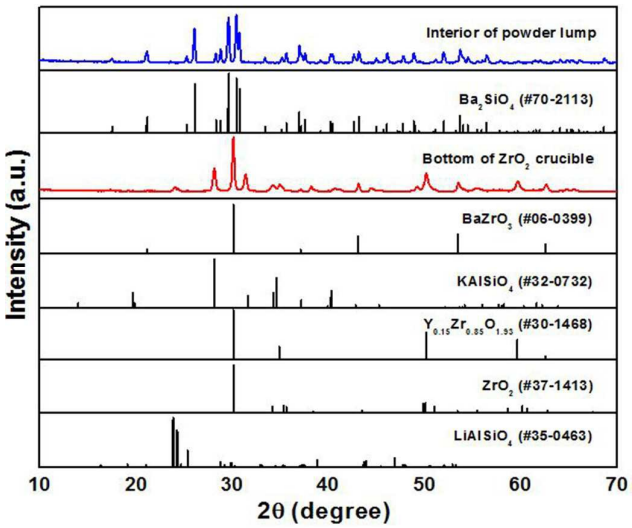

Fig. 8 XRD patterns of Ba_2SiO_4:($Li_{0.02}$,$Eu_{0.02}$) phosphor (Li = 300% excess) synthesized using zirconia crucible.

Table 1 Li Contents of Ba_2SiO_4:(Li_x,$Eu_{0.02}$) Determined by ICP.

Li (x)	Li content, ppm (nominal composition, ppm)	Li defect ($\times 10^{-2}$)
0.02	1.06 (380.93)	1.99
0.05	41.49 (962.6)	4.75
0.08	155.63 (1557.16)	7.20

intensity is increased with higher Li^+ concentration, and the maximum intensity at Li = 0.02 is observed, indicating that the optimal concentration of Li^+-ion is 0.02. It should be mentioned that the defect-related luminescent materials have been prepared and characterized, such as nanocrystal SiO_2,[23] MoS_2,[24] Gd_2O_3:Dy,[25] ZnO quantum dots,[26] Y_2O_3:Eu^{27} etc. As shown in Table 1, the considerable amounts of Li-defects are observed due to the volatility of Li_2O in the firing step at 1250℃. It is presumed that the cationic defects induced by the Li^+-ions introduced into the Ba^{2+}-sites have an effect on the effective energy transfer from the host-lattice (Ba_2SiO_4) to the Eu^{2+}-activator ions as revealed in the diffuse reflectance spectra (Fig. 6). For the Ba_2SiO_4:(Li_x,$Eu_{0.02}$) phosphor materials, the maximum emission intensity corresponds to the optimal concentration of Li^+-ion (x = 0.02). It is remarkable that the emission intensity of Ba_2SiO_4:($Li_{0.02}$,$Eu_{0.02}$) phosphor is about 3.2 times higher than that of Ba_2SiO_4:$Eu_{0.02}$ phosphor even in very small quantity of Li. Fig. 6 presents the diffuse reflectance spectra of Ba_2SiO_4, Ba_2SiO_4:$Eu_{0.02}$, and Li-codoped Ba_2SiO_4:$Eu_{0.02}$ phosphors. As the Eu^{2+} ions are doped into the Ba_2SiO_4 host lattice, the broad absorption bands are manifested in the range of 300-450 nm. It might be assured that the broad absorption bands around 300 and 450 nm in Ba_2SiO_4:Eu^{2+} phosphor are associated with the 4f →5d transition of Eu^{2+} because the absorption band of the Ba_2SiO_4 host material is absent in this wavelength range. Furthermore, the absorption bands of the Li-doped Ba_2SiO_4:$Eu_{0.02}$ are still stronger than that of Ba_2SiO_4:$Eu_{0.02}$ without Li-doping, which is well coincident with the excitation spectra as previously presented in Fig. 5.

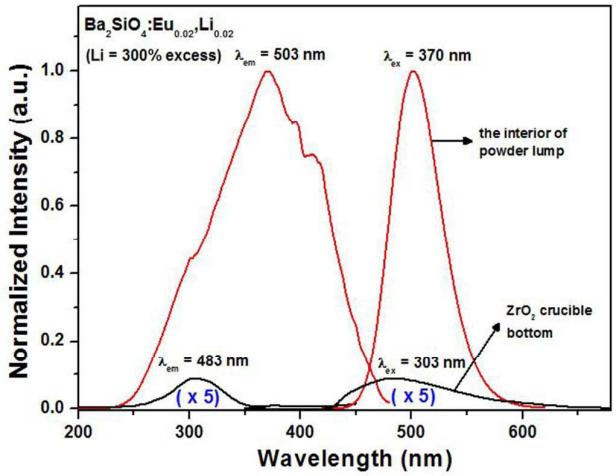

Fig. 9 Excitation and emission spectra of Ba_2SiO_4:($Li_{0.02}$,$Eu_{0.02}$) phosphor (Li = 300% excess) synthesized using zirconia crucible.

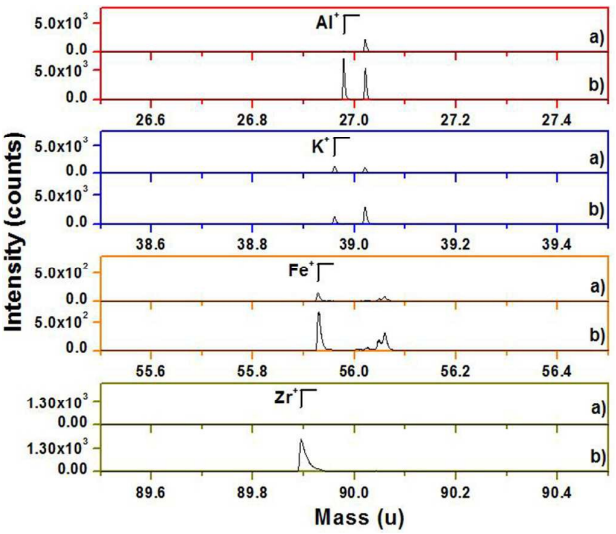

Fig. 10 TOF-SIMS mass spectra of Ba_2SiO_4:($Li_{0.02}$,$Eu_{0.02}$) synthesized using Li-300% excess. In each secondary ion, the spectrum in the upper part (a) corresponds to the powder sample and that in the lower part (b) corresponds to the bottom of the zirconia crucible.

The remarkable PL enhancement by Li-codoping warrants further examination of the materials in search for its origin. One may presume that the Li^+ ions introduced into the Ba^{2+}-sites in Ba_2SiO_4:$Eu_{0.02}$ crystal lattice create the cation vacancies as well as the oxygen vacancies for charge balance, which might act as a sensitizer for the effective energy transfer from the host lattice (Ba_2SiO_4) to the activator ions (Eu^{2+}). As shown in Table 1, ICP results indicate that the materials do have a considerable amount of Li defects probably due to the volatility of Li_2O in the firing step, at 1250℃ for 12h in air and 4% H_2/Ar. In contrast to our expectation, however, the increase in the nominal content of Li improves the PL of Ba_2SiO_4:($Li_{0.02}$,$Eu_{0.02}$) synthesized using the excess Li_2CO_3 (100%, 200%, and 300%) as shown in Fig. 7. Namely, the PL intensity is much higher when the samples were prepared with an excess amount of Li_2CO_3, indicating that the presence of the Li defects is not the critical cause for the PL enhancement. In understanding the origin of the PL enhancement, a critical clue is evident in TOF-SIMS results for the Ba_2SiO_4:($Li_{0.02}$,$Eu_{0.02}$) (Li = 300% excess) product which was synthesized using SiO_2 (99.6% purity), $BaCO_3$ (99% purity), Li_2CO_3 (99.99% purity), and Eu_2O_3 (99.9% purity). After firing, two different samples were collected in the zirconia crucible, in first the interior of the cohesive powder-lump, in second the fused part remained at the bottom of the zirconia crucible. XRD pattern of the powder in the interior of the powder-lump shows that of Ba_2SiO_4 with a pure single phase, whereas the impurity phases such as $BaZrO_3$, $LiAlSiO_4$, $KAlSiO_4$, and ZrO_2 are manifested at the bottom of zirconia crucible as presented in Fig. 8. The PL properties between two samples are compared in Fig. 9. The excitation and emission spectra of the impurity phases at the bottom of zirconia crucible are quite different from those of Ba_2SiO_4:Eu^{2+} and its intensities are very low. Fig. 10 presents TOF-SIMS positive secondary ion mass spectra of the two samples. Interestingly, three main impurities determined by ICP-MS (see Table S1) are present much more significantly in the sample from the bottom. Moreover, the Zr^+ secondary ion is present only in the sample from the bottom, whereas there is no Zr^+ ion in the sample from the upper part. Fig. 11 shows the images of the Al^+, K^+, Fe^+, and Zr^+ secondary ion in which the specific elemental topography of each ion in the samples are presented in a linear color scale bar with color range from black to white, where black corresponds to the zero counts and white to the maximum intensity (e.g. 2.972×10^3 counts for Al^+ at the left in the top in Fig. 11). Images of TOF-SIMS collected from the different positions of the powder sample coincide well with the intensities of the secondary cations as presented in Fig. 11. It should be noted that the intensities of the secondary cation in the sample collected from the bottom of the crucible are still stronger than those from the upper part. Since the target product particles remain in the upper part of the crucible, it is reasonable to say that the products have impurities much less than what we would expect from the amount of the impurities of the starting precursors and that the added Li_2CO_3 as a Li^+ ion source effectively removes the impurities in the precursors. This is supported by the fact that in Fig. 7 all the products prepared with excess Li_2CO_3 (100, 200 and 300%) show nearly the same PL intensity. It should be noted that the liquid-phase sintering is usually considered to occur in three stages which are rearrangement, solution precipitation, and Ostwald ripening.[28] As the temperature is raised above 710℃, the Li_2CO_3-Li_2O mixture melts and reacts with $BaCO_3$, SiO_2, and Eu_2O_3 to form a eutectic liquid. Assuming that there is good wetting between the liquid and the particulate solids, the impure solids dissolve at the solid/liquid interfaces, diffuse through the liquid and precipitate on the particles at another site which is the bottom of the zirconia crucible in our system. In essence, the excess amount of Li_2CO_3 as a Li^+-source plays an important role as a molten flux medium that effectively traps impurities in the melt and thus result in a low impurity level in the phosphor product. This proposition is further substantiated when we

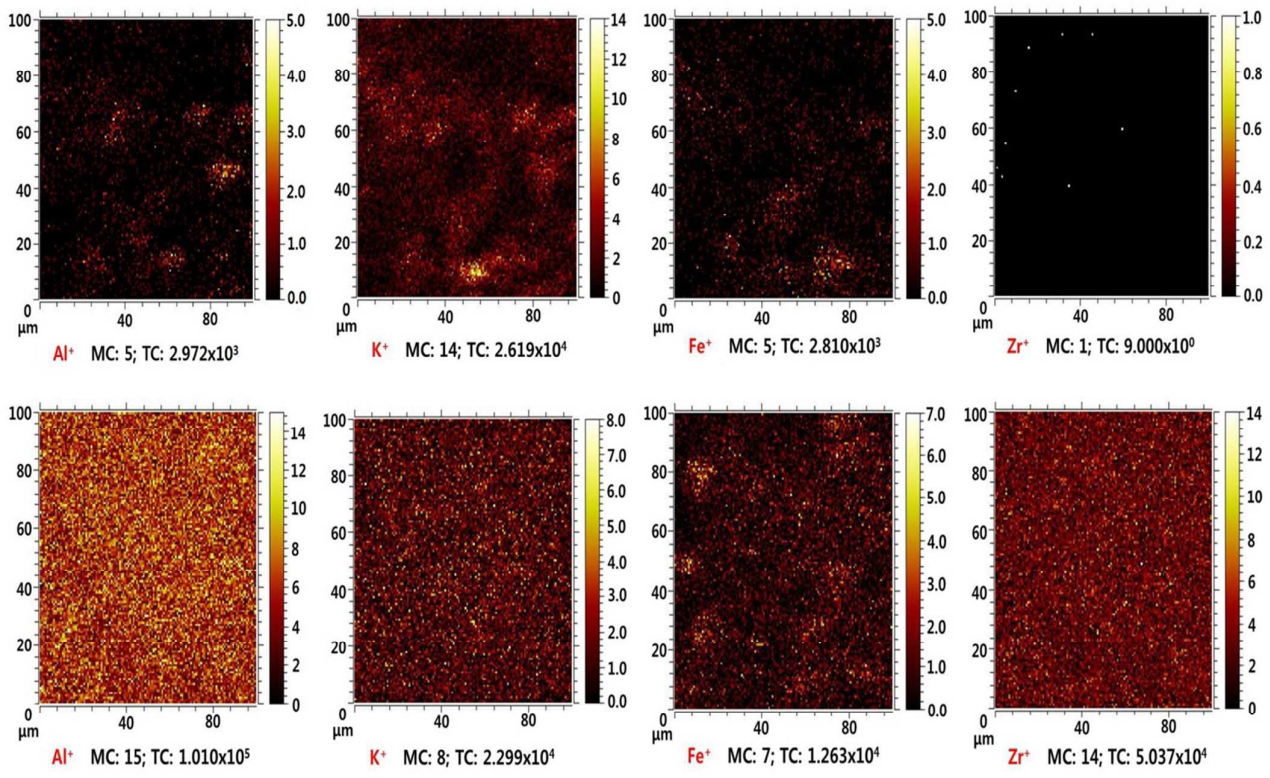

Fig. 11 TOF-SIMS images of Ba_2SiO_4:($Li_{0.02}$,$Eu_{0.02}$) synthesized using Li-300% excess. The images in the upper part correspond to the powder sample and those in the lower part correspond to the bottom of the zirconia crucible.

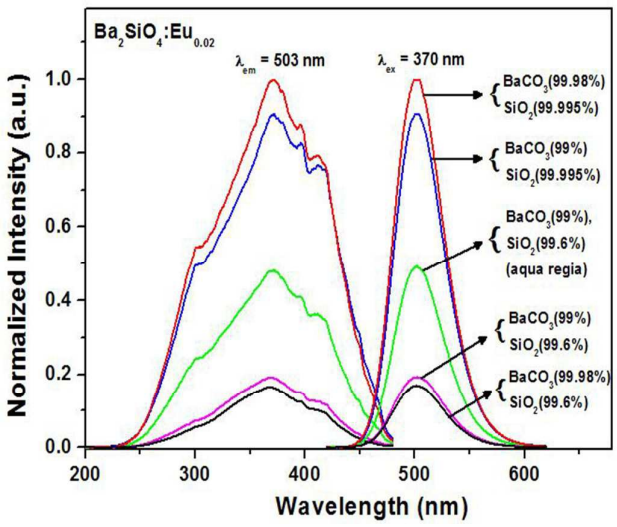

Fig. 12 PL spectra of Ba_2SiO_4:$Eu_{0.02}$ synthesized using the starting chemicals with the high and low purity.

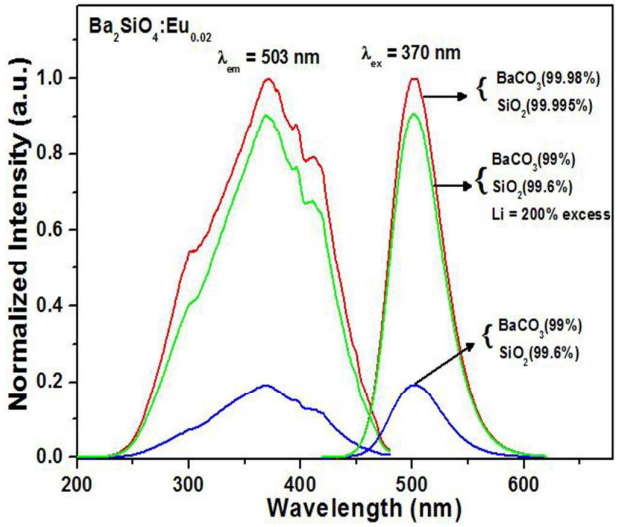

Fig. 13 Comparison of PL property between Ba_2SiO_4:$Eu_{0.02}$ (using the high purity) and Ba_2SiO_4:($Li_{0.02}$,$Eu_{0.02}$) (using the low purity and Li-200% excess).

compare the PL intensities of the Li-codoped products with another set of products prepared without Li-codoping but instead with high-purity precursors. Fig. 12 shows the excitation and emission spectra of Ba_2SiO_4:$Eu_{0.02}$ products with precursors of varied purities. From the trend in the PL intensity, it is evident that the PL efficiency is strongly dependent of the chemicals purities of the precursors, with the maximum emission intensity from the highest-purity $BaCO_3$ (99.98%) and

Table 2 Luminescent Properties of Ba_2SiO_4:($Li_{0.02}$,$Eu_{0.02}$) Phosphor Materials.

Starting material	Maximum I_{em} ratio (%)[a]	Emission peak area ratio (%)[a]	Relative brightness, cd/m^2 (%)[a]	Quantum Yield (%)
$BaCO_3$(H)[b], SiO_2(H)[b] No-Li addition	100	100	100	63.9
$BaCO_3$(L)[b], SiO_2(L)[b] Li : 200% excess	90.8	91.4	92.6	69.0
$BaCO_3$(L)[b], SiO_2(L)[b] Li : 300% excess	88.4	88.8	91.3	63.2
$BaCO_3$(L)[b], SiO_2(L)[b] Li : No-excess	60.9	61.7	63.2	53.9
$BaCO_3$(L)[b], SiO_2(L)[b] No-Li addition	19.3	19.5	22.3	31.5

[a] Property of Ba_2SiO_4:$Eu_{0.02}$ material synthesized with $BaCO_3$(H) and SiO_2(H) is located to 100%.

[b] $BaCO_3$(H) corresponds to $BaCO_3$(99.98% purity), SiO_2(H) to SiO_2(99.995% purity), $BaCO_3$(L) to $BaCO_3$(99% purity), and SiO_2(L) to SiO_2(99.6% purity).

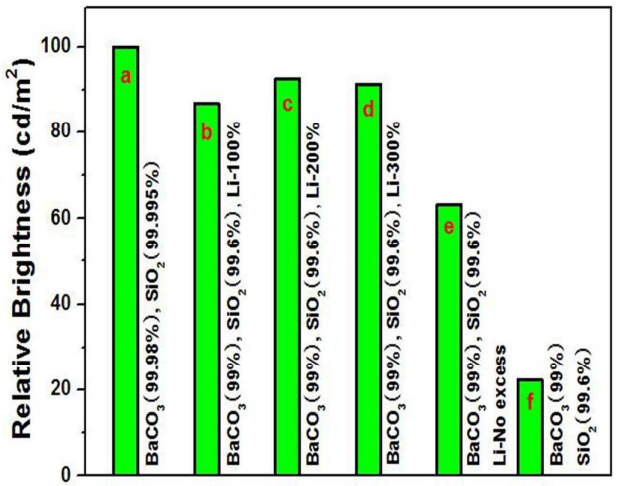

Fig. 14 Relative brightness of Phosphor Materials; Ba_2SiO_4:$Eu_{0.02}$ (a), Ba_2SiO_4:($Li_{0.02}$,$Eu_{0.02}$) (b), Ba_2SiO_4:($Li_{0.02}$,$Eu_{0.02}$) (c), Ba_2SiO_4:($Li_{0.02}$,$Eu_{0.02}$) (d), Ba_2SiO_4:($Li_{0.02}$,$Eu_{0.02}$) (e), Ba_2SiO_4:$Eu_{0.02}$ (f). Brightness of Ba_2SiO_4:$Eu_{0.02}$ (a) is located to 100%.

SiO_2 (99.995%) precursors being 5.2 times higher than that from the lowest-purity $BaCO_3$ (99%) and SiO_2 (99.6%) precursors. The emission intensity from $BaCO_3$ (99%) and SiO_2 (99.995%) precursors is 4.7 times higher than that from $BaCO_3$ (99%) and SiO_2 (99.6%), indicating that the emission intensity is more sensitive to the purity of SiO_2 than that of $BaCO_3$. A Ba_2SiO_4:$Eu_{0.02}$ product prepared with the aqua regia-purified SiO_2 and $BaCO_3$ (99%) shows a PL intensity 2.5 times higher than that of Ba_2SiO_4:$Eu_{0.02}$ using $BaCO_3$ (99%) and the as-received SiO_2 (99.6%). Remarkably, Fig. 13 shows that the PL intensities are quite comparable between Li-codoped Ba_2SiO_4:($Li_{0.02}$,$Eu_{0.02}$) synthesized using the lowest-purity $BaCO_3$ (99%) and SiO_2 (99.6%) but with 200%-excess Li_2CO_3, and Ba_2SiO_4:$Eu_{0.02}$ synthesized using the highest-purity $BaCO_3$ (99.98%) and SiO_2 (99.995%) precursors. As shown in Table S1, further ICP-MS analysis showed that the low-purity SiO_2 (Aldrich, 99.6% purity) contain three main impurities: Al (3891 ppm), K (1312 ppm), and Fe (478 ppm). After treating the SiO_2 with a hot aqua regia, the concentrations of three main impurities are also reduced: Al (2288 ppm), K (186 ppm), and Fe (102 ppm). Fig. 14 shows the relative brightness monitored under 365 nm UV-light, which is in good agreement with PL results as presented in Fig. 7 and Fig. 13. Luminescent properties obtained from the emission spectra and quantum yields of Ba_2SiO_4:$Eu_{0.02}$ phosphor materials before and after Li-doping are summarized in Table 2. The photoluminescence quantum yield (QY), which is the probability that a chromophore emits a photon upon its return from the excited to the ground state, can be represented as the ratio of its radiative to the non-radiative rate,[29-32]

$$\Phi = k_{rad} / (k_{rad} + k_{nrad}) \quad (1)$$

where k_{rad} and k_{nrad} are the rate constant for radiative emission and non-radiative deexcitation to the ground state, respectively. As presented in Table 2, the luminescent properties (maximum I_{em} ratio, emission peak area ratio, and relative brightness) associated with the radiative process have the similar values, while the QY values (related with radiative and non-radiative process) are somewhat different, i.e., the smaller differences compared to those of radiative process. Evidently, the discrepancy between three-radiative and QY values may be attributed to the energy losses due to the non-radiative process.

4 Conclusions

Large photoluminescence enhancement up to 470% has been achieved for the green emitting $(Ba,Sr)_2SiO_4:Eu^{2+}$ phosphor material via Li-codoping using Li_2CO_3 as a flux, when low-purity precursors were employed. By examining the elemental distribution in the reaction products and flux after the Li-codoping experiment, it was discovered that the excess Li condition results in extraction of Al, K and Fe impurities from the low-purity precursors, hence decreasing impurity concentrations in the phosphor product. This effect was further verified by comparing the photoluminescence efficiency of the Li-codoped phosphors with that of Li-undoped phosphors that were prepared with high-purity precursors. This newly-discovered mechanism of photoluminescence enhancement upon Li-codoping may lead to more economical adoption of solid state lighting for energy efficiency. This also provides an

efficient synthetic route aiming alleviation of the undesired luminescent quenching by impurities and thus allows us to explore new phosphors that are particularly susceptible to such impurity effect.

Acknowledgements

This research was financially supported by the Ministry of Education (MOE) and National Research Foundation of Korea (NRF) through the Human Resource Training Project for Regional Innovation (2014H1C1A1066859).

References

1 G. Chen, H. Liu, H. Liang, G. Somesfalean and Z. Zhang, *J. Phys. Chem. C*, 2008, **112**, 12030-12036.
2 D. Li, Y. Wang, X. Zhang, H. Dong, L. Liu, G. Shi and Y. Song, *J. Appl. Phys*., 2012, **112**, 094701-094705.
3 Q. Sun, X. Chen, Z. Liu, F. Wang, Z. Jiang and C. Wang, *J. Alloys Compd*., 2011, **509**, 5336-5340.
4 Y. Wang, N. Can and P. D. Townsend, *J. Lumin*., 2011, **131**, 1864-1868.
5 J. C. Park, H. K. Moon, D. K. Kim, S. H. Byeon, B. C. Kim and K. S. Suh, *Appl. Phys. Lett*., 2000, **77**, 2162-2164.
6 S. H. Byeon, M. G. Ko, J. C. Park and D. K. Kim, *Chem. Mater*., 2002, **14**, 603-608.
7 F. Gu, S. F. Wang, M. K. Lu, G. J. Zhou, D. Xu and D. R. Yuan, *Langmuir*., 2004, **20**, 3528-3531.
8 S. H. Shin, J. H. Kang, D. Y. Jeon and D. S. Zang, *J. Lumin*., 2005, **114**, 275-280.
9 W. Li and J. Lee, *J. Phys. Chem. C*, 2008, **112**, 11679-11684.
10 C. Zhang, H. Lian, D. Kong, S. Huang and J. Lin, *J. Phys. Chem. C*, 2009, **113**, 1580-1588.
11 H. K. Yang, J. W. Chung, B. K. Moon, B. C. Choi, J. H. Jeong, J. S. Bae and K. H. Kim, *Solid State Sci*., 2011, **13**, 1420-1423.
12 E. L. Cates, A. P. Wilkinson and J. H. Kim, *J. Phys. Chem. C*, 2012, **116**, 12772-12778.
13 S. Shionoya and W. Yen, Phosphor Handbook, CRC Press, London, New York, 1999, 192.
14 H. S. Kang, S. K. Hong, Y. C. Kang, K. Y. Jung, Y. G. Shul and S. B. Park, *J. Alloys Compd*., 2005, **402**, 246-250.
15 H. P. Grosse and E. Tillmanns, *Cryst. Struct. Commun*., 1974, **3**, 599-601.
16 A. V. Walker, *Anal. Chem.,* 2008, **80**, 8865-8870.
17 S. Seki, H. Tamura and H. Sumiya, *Appl. Surf. Sci*., 1999, **147**, 14-18.
18 S. Zhang, Y. Nakai, T. Tsuboi, Y. Huang and H. J. Seo, *Chem. Mater*., 2011, **23**, 1216-1224.
19 W. B. Im, Y. I. Kim, H. S. Yoo and D. Y. Jeon, *Inorg. Chem*., 2009, **48**, 557-564.
20 K. Inoue, N. Hirosaki, R. J. Xie and T. Takeda, *J. Phys. Chem.* C, 2009, **113**, 9392-9397.
21 D. Kim, J. Jang, S. I. Ahn, S. H. Kim and J. C. Park, *J. Mater. Chem. C,* 2014, **2**, 2799-2805.
22 D. Kim, S. Park, S. Kim, S. G. Kang and J. C. Park, *Inorg. Chem*., 2014, **53**, 11966-11973.
23 K. S. Min, K. V. Shcheglov, C. M. Yang, H. A. Atwater, M. L. Brongersma and A. Polman, *Appl. Phys. Lett*., 1996, **69**, 2033-2035.
24 P. K. Chow, R. B. Jacobs-Gedrim, J. Gao, T.M Lu, B. Yu, H. Terrones and N. Koratkar, *ACS Nano*, 2015, **9**, 1520-1527.
25 T. Selvalakshmi, S. Sellaiyan, A. Uedono and A. C. Bose, *RSC Adv*., 2014, **4**, 34257-34266.
26 A. Asok, A. R. Kulkarni and M. N. Gandhi, *J. Mater. Chem. C*, 2014, **2**, 1691-1697.
27 H. Huang, X. Sun, S. Wang, Y. Liu, X. Li, J. Liu, Z. Kang and S. T. Lee, *Dalton Trans*., 2011, **40**, 11362-11366.
28 M. N. Rahaman, *Ceramic Processing and Sintering,* Marcel Dekker, New York, 1995.
29 J. R. Lakowicz, Principles of Fluorescence Spectroscopy, 3rd ed. Springer: New York, 2006.
30 M. Yorulmaz, S. Khatua, P. Zijlstra, A. Gaiduk and M. Orrit, *Nano Lett*., 2012, **12**, 4385−4391.
31 J. Zhao, O. Chen, D. B. Strasfeld and M. G. Bawendi, *Nano Lett*., 2012, **12**, 4477−4483.
32 J. Hoy, P. J. Morrison, L. K. Steinberg, W. E. Buhro and R. A. Loomis, *J. Phys. Chem. Lett*., 2013, **4**, 2053−2060.

Table of contents (Graphical Abstract)

The emission intensity of Ba_2SiO_4:($Li_{0.02}$,$Eu_{0.02}$) (200% excess Li) synthesized using low purity precursors (99%-pure $BaCO_3$ and 99.6%-pure SiO_2), is found to be 470% as high as that of Ba_2SiO_4:$Eu_{0.02}$ (no-Li). The excess Li_2CO_3 autonomously removes the impurities that were originally contained in the low purity precursors, in particular SiO_2, and thus critically improves the photoluminescence efficiency of the material.